

Surface Extraction in Coherence Scanning Interferometry by Gauss-Markov Monte-Carlo Method and Teager-Kaiser Operator

Fabien Salzenstein¹ and Abdel-Ouahab Boudraa² ^a

¹Université de Strasbourg, Laboratoire ICube, 23 Rue du Loess, Strasbourg, 67037 Cedex 2, France

²Ecole Navale/Arts et Metiers Institute of Technology, IRENav, BCRM Brest, CC 600, Brest, France


Keywords: AM-FM Model, Teager-Kaiser Energy Operator, Gauss-Markov Process, Rugosity, Surface Extraction.

Abstract: This work deals with the problem of surface extraction using a combination of Teager-Kaiser operators and Gauss-Markov process in the context of coherence scanning (or white light scanning i.e. WLSI) interferometry. Our approach defines a Markov sequence along multiple surface profiles extracting their characteristics by the means of parameters describing the fringe signals along the optical axis, while most studies of the literature are restricted to local extraction of signals in one-dimensional mode. Thus the interest of the proposed strategy is to classify different surfaces present in a material, in particular the information relating to their roughness, by exploiting the statistical dependence between neighboring points where the noise is supposed to be white Gaussian noise. The effectiveness of our unsupervised method is illustrated on both synthetic and real images.

1 INTRODUCTION

White light scanning interferometry (WLSI) technique, has shown efficiency for computing surface depth measurements, and specifically estimating their roughness. A high precision is required in order to control the fabrication techniques of new materials, microelectronic devices and MicroElectroMechanical Systems (MEMS) (O'Mahony et al., 2003). Moreover, the strength of the WLSI technique lies in its ability to provide fast, robust and high resolution measurements, using methods based on the AM-FM signal model representing variations in light intensity measured along the optical axis of an interference microscope. According to this model, the height of the surface material is simultaneously contained within the envelope and the phase of the modulated signal. An efficient method to extract the surface position, by detecting the envelope peak, is the so called five sample adaptive technique which uses only five adjacent samples along the optical axis (Larkin, 1996). Other signal processing tools such as the Fourier transform (de Groot et al., 2002), the windowed Fourier transform (WFT) (Ma et al., 2011) or the continuous wavelet transform (CWT) (Sandoz, 1997; Li et al., 2008) have also been exploited in WLSI. Based on these transformations, phase retrieving strategies

have been developed for zero optical path difference (ZOPD) compensation by extracting the local maxima (ridge detection) of the CWT (resp. WFT). For example, the CWT and the WFT are used to compute the phase information at a local maximum, and have been applied to fringe pattern analysis (Niu et al., 2009; Kemao, 2004). Due to its implementation simplicity, effectiveness, and adaptation of the AM-FM signal model, the nonlinear Teager-Kaiser energy operator (TK or TKEO) is a well suited tool in this domain. This operator allows a fast and local demodulation of signals modeled by AM-FM functions extracting the instantaneous envelope and frequency. Maragos and Bovik extended this energy operator to signals of higher dimensions rendering it applicable to real-valued grayscale images as a 2D operator (Maragos and Bovik, 1995). A higher order differential energy operators, for 1D signals, has been introduced by Maragos and Potamianos (Maragos and Potamianos, 1995). This work has been extended by introducing a large class of operators for both 1D signals (Salzenstein et al., 2007) followed by their multidimensional version (Salzenstein et al., 2013). On the other hand, if these different operators efficiently estimate the surfaces contained in an observed piece of material, they are not well efficient for surfaces recognition due to both problems: a follow-up of the surfaces, and their correct estimation, specifically in the presence of close surfaces. In order to solve these

^a  <https://orcid.org/0000-0002-1864-2859>

challenges, we combine TKEO with a Markovian approach, by drawing on the spectral tracking carried out in the field of astronomy, where some works provide solutions to similar problems, although the signals do not contain an additional carrier term, by exploiting Bayesian approaches using MCMC (Monte Carlo Markov Chain) algorithms (Mazet et al., 2015). The Bayesian methodology provides a rich framework for modeling inverse problems and allows us to define a surface decomposition and pursuit approach. To the best of our knowledge, the problem of the decomposition of multiple surfaces related to WLSI interferometric images has not been addressed in the literature using MCMC based on Gauss-Markov model applied on different characteristics related to each surface. More precisely we describe all surfaces through their characteristic parameters such as envelope, frequency, amplitude and variance, based on a Gaussian envelope model added to a carrier, in order to regularize and better discriminate them. In reference (Hissmann and Hamprecht, 2005; Zou et al., 2016) Bayesian approaches has been proposed as a post-processing, to eliminate outliers or to denoise a single surface, introducing prior knowledge on the roughness of the surface, but without Markovian modeling of the multiple fringe characteristics, that we introduce in this study. In reference (Gurov and Volynsky, 2012) a Kalman filter has been used to process fringes along the optical axis of each slice, whereas a Markov regularization to the phase of interferometric images has been applied in (Wu and Boyer, 2011). Let us summarize the main contributions of our study, in the specific field of the WLSI interferometric imaging.

- The first contribution consists in exploiting a TK algorithm to classify the surfaces i.e. by grouping sites belonging to an identical surface areas, using distance neighborhood criteria;
- The second contribution consists in introducing an unsupervised MCMC method combined with a Gauss-Markov model applied on characteristics related to the fringe signal, in order to better regularize the surfaces, and estimate their roughness;
- The third contribution consists in exploiting an information compression algorithm to initialize the MCMC method, in the context of close surfaces. This amounts to extend the surfaces characteristics in an area suspected of containing adjacent trajectories, in particular where TKEO fails.
- The fourth contribution, inspired by the work of Mazet al. (Mazet et al., 2015), consists of randomly testing, in the MCMC procedure, the belonging of each site to the different surfaces according to a distance criterion including the gra-

dent matrices. This allows the nearby surfaces to be processed more effectively.

The remainder of the paper is organized as follows: after the presentation of the context of the interferometric data in section 2 we introduce TK algorithm in section 3 followed by the Gauss-Markov approach adapted to the studied problem in section 4. Unsupervised MCMC approach is detailed in section 5. Finally, results on both synthetic and real images are presented section 6. Let us notice that in this study, the surfaces are sometimes called 'trajectories'.

2 INTERFEROMETRIC SIGNAL

A series of images is acquired with a camera at regular intervals to give a stack of xyz images. For polychromatic interferometry, the total intensity is the sum of the interferences at each wavelength. From the given interferometric fringe signals, the objective consists in extracting the position of the analyzed surface(s). A typical intensity signal obtained from a digital camera as the OPD is varied in the interferometer at a given point (x, y) on the material surface, can be approximated along the optical z -axis by a modulated sinusoid as follows (Larkin, 1996):

$$s(x, y, z) = a(x, y, z) + b(x, y) \underbrace{\exp \left[- \left(\frac{z - h(x, y)}{l_c} \right)^2 \right]}_{C(x, y, z)} \times \cos \left[\frac{4\pi}{\lambda_0} (z - h(x, y)) + \alpha(x, y) \right]$$

where z is a vertical scanning position along the optical axis, $h(x, y)$ represents the height of the surface, $a(x, y, z)$ is an offset intensity containing low frequency components, $b(x, y)$ is a factor proportional to the reflected beam intensity, and $\alpha(x, y)$ is an additional phase offset and $C(x, y, z)$ is the envelope. The parameter l_c represents the coherence length of the light source and λ_0 is the average wavelength of the light source. Generally the phase offset varies slowly from one point (x, y) to the next, and can be neglected, since only relative heights of the surface matter. The main challenge consists in determining the height at each point of the surface by exploiting the information provided by both the envelope and the phase simultaneously. Most algorithms, whether based on envelope detection (Larkin, 1996; Sandoz, 1997), frequency domain analysis (de Groot and Deck, 1993; de Groot et al., 2002), correlation with a reference fringe (Chim and Kino, 1990), Hilbert transformation (Pavliček and Michalek, 2012), TK algorithm (Gianto

et al., 2016), extraction of the phase information (Guo et al., 2011) or Kalman approach (Gurov et al., 2004), proceed along the optical axis, for each lateral position (x, y) . Some 2D techniques have been proposed (Gurov and Volynsky, 2012; Zhu and Wang, 2012). In our study, we perform 2D processing data, based on a 1D initialization. The Figure 1 represents an interferometric signal in biological imaging, along the optical axis. The numbered vertices indicate superimposed surfaces of materials.

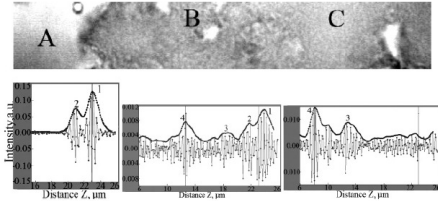


Figure 1: Mineral component of the phosphate family.

3 TK ENERGY OPERATORS

TKEOs based demodulation algorithms (Boudraa and Salzenstein, 2018) are efficient non-linear and local methods for envelope detection and phase retrieval from AM-FM signals such as those given by Eq. (1). The output of the continuous 1D TKEO, noted Ψ , for a real-valued signal $s(t)$ is given by:

$$\Psi[s(t)] = [\dot{s}(t)]^2 - s(t)\ddot{s}(t) \quad (1)$$

where $\dot{s}(t)$ and $\ddot{s}(t)$ denote the first and the second time derivatives of $s(t)$ respectively. Under realistic conditions (Maragos et al., 1993), when applied to AM-FM signal $s(t) = a(t)\cos(\phi(t))$, the 1D TKEO yields as output $\Psi[s(t)] \approx [a(t)\dot{\phi}(t)]^2$. Thus the local envelope $a(t)$ and the instantaneous frequency $\dot{\phi}(t)$ can be estimated using the energy separation algorithm (ESA) (Maragos et al., 1993):

$$|\dot{\phi}(t)| \approx \sqrt{\frac{\Psi[\dot{s}(t)]}{\Psi[s(t)]}}; |a(t)| \approx \frac{\Psi[s(t)]}{\sqrt{\Psi[\dot{s}(t)]}} \quad (2)$$

Positivity conditions of this operator has been studied in (Préaux et al., 2022). Extension to signals of higher dimensions, rendering it applicable to real-valued gray level images $I(x_1, x_2)$ as a 2D TKEO:

$$\Phi[I(x_1, x_2)] = \|\nabla I(x_1, x_2)\|^2 - I(x_1, x_2)\nabla^2 I(x_1, x_2) \quad (3)$$

In a similar manner to the 1D TKEO, for a narrowband image $I(x_1, x_2) = a(x_1, x_2)\cos(\phi(x_1, x_2))$ the output of the 2D TK is given by $\Psi[x_1, x_2] \approx [a(x_1, x_2)\dot{\phi}(x_1, x_2)]^2$. The spatially-varying amplitude $a(x_1, x_2)$ can be interpreted as modeling local image

contrast and the instantaneous frequency $\omega(x_1, x_2) = \nabla\phi(x_1, x_2)$ describes locally energy spatial frequencies. Combining all energies, yields the 2D ESA (Maragos and Bovik, 1995), where $x_i \in \{x_1, x_2\}$:

$$|\omega_{x_i}(x_1, x_2)| \approx \frac{\Phi[I(x_1, x_2)]}{\sqrt{\Phi\left[\frac{\partial I(x_1, x_2)}{\partial x_i}\right]}}$$

$$|a(x_1, x_2)| \approx \frac{\Phi[I(x_1, x_2)]}{\sqrt{\Phi\left[\frac{\partial I(x_1, x_2)}{\partial x_1}\right] + \Phi\left[\frac{\partial I(x_1, x_2)}{\partial x_2}\right]}}$$

The FSA method (Larkin, 1996) used in WLSI, corresponds to the discrete TKEO, applied to a differentiated signal. The 2D TKEO has shown its efficiency for image demodulation and particularly for local envelope extraction (Maragos and Bovik, 1995; Boudraa et al., 2005; Larkin, 2005). This operator has been extended to multidimensional signals using directional derivatives (Salzenstein et al., 2013). In (Salzenstein et al., 2014), a combination of 1D TKEO using a correlation approach by means of the flexible operator Ψ_B (Boudraa et al., 2008) was proposed, in order to improve the resolution of surfaces extracted in a context of WLSI images.

4 PROPOSED GAUSS-MARKOV MODEL

We process the volume of data, described in section 2 by proceeding slice by slice, corresponding to 2D signals $s(x, z)$ say of size $N \times M$ where M is the length of the optical axis z and N is the maximum size of the lateral axis x . To do this, we propose to introduce a Markovian model consisting of an extension of the scheme introduced in (Mazet et al., 2015) by taking into account the carrier terms, as follows:

$$s(x, z) = \sum_{k=1}^K \sum_{n=n_k}^{N_k} a_{k,n} \exp\left[-\frac{(z - c_{k,n})^2}{2\sigma_{k,n}^2}\right] \times \cos(2\pi\nu_{k,n}(z - c_{k,n}) + \alpha_k) \delta_{n,x}$$

We note by $S_k = \{c_{k,n_k}, c_{k,n_k+1}, \dots, c_{k,N_k}\}$ a set of the centers of a "surface" which is seen as a 1D trajectory in the 2D plane corresponding to the centers $c_{k,n}$ of the peaks. The n th peak of class k is parameterized by its center $c_{k,n}$, amplitude $a_{k,n}$ and with (or standard deviation) $\sigma_{k,n}$. The Kronecker delta $\delta_{n,x}$ equals 1 if $n = x$ and 0 otherwise; it codes the presence or the absence of the n th peak of class k . The observed signal $f(x, y)$ is a noisy version of $s(x, y)$:

$$f(x, z) = s(x, z) + b(x, z) \quad (4)$$

where $b(x, y)$ is a Gaussian white noise modeled as:

$$b(x, z) \sim \mathcal{N}(0, \sigma_b) \quad (5)$$

Let (x, z) be the spatial coordinates of an image. The information to be extracted from the image is described by four parameters namely as the amplitude of the Gaussians $a_{k,n}$, their mean values $c_{k,n}$, their standard variances $\sigma_{k,n}$, as well as the frequency associated with the local carriers $v_{k,n}$. We make assumption that this set of parameters $(a_{k,n}, c_{k,n}, \sigma_{k,n}, v_{k,n})$ follows a priori 1D Gauss-Markov type probabilistic laws:

$$\forall k \quad c_{k,n} \sim \mathcal{N}(c_{k,n-1}, r_c) \quad (6)$$

where parameter r_c provides an indication related to the roughness of the surface. Finally

$$\begin{aligned} p(\mathbf{c}_k | r_c, l_k) &\propto p(c_{k,n_k}) \prod_{n=n_k+1}^{N_k} p(c_{k,n} | c_{k,n-1}, r_c, l_k) \\ &\propto p(c_{k,n_k}) \frac{1}{(2\pi r_c)^{(l_k-1)/2}} \exp\left(-\frac{\|\mathbf{D}\mathbf{c}_k\|^2}{2r_c}\right) \end{aligned}$$

where \mathbf{D} represents a gradient matrix and $l_k = N_k - n_k + 1$ the length of a surface i.e., the number of points describing it. Let us notice, in the formula (7) the vector \mathbf{c}_k owns a size $l_k \times 1$ and the matrix \mathbf{D} , $(l_k - 1) \times l_k$. The matrix $\mathbf{D}\mathbf{c}$ is therefore a column vector of the differences between two adjacent peaks. The peaks are considered to be mutually independent knowing r_c and l :

$$p(\mathbf{c} | r_c, l) = \prod_{k=1}^K p(c_k | r_c, l_k) \quad (7)$$

Unlike to the approach in reference (Mazet et al., 2015), we do not make any assumption about the prior probability $p(c_{k,n_k})$, described there as uniform distribution, because we combine the previous model with a TK deterministic method. We define amplitudes, variances and frequencies in the same way:

$$\lambda_{k,n} \sim \mathcal{N}(\lambda_{k,n-1}, r_\lambda)$$

where $\lambda_{k,n} \in \{a_{k,n}, c_{k,n}, \sigma_{k,n}, v_{k,n}\}$. Here again, it will not be necessary to adjust the prior probabilities $p(a_{k,n_k})$, $p(\sigma_{k,n_k})$, $p(v_{k,n_k})$ because we initialize these parameters by the means of TK function. We assume that these random variables are independent conditional on the observation.

5 TK-MCMC ALGORITHM

Let $\mathbf{f} = [f(n, m)]_{1 \leq n \leq N, 1 \leq m \leq M}$ be the noisy data. Using the Bayes rule leads to the following global posterior density, related to the prior deterministic parameter $\theta = (\sigma_b, r_c, r_a, r_w, l_v)$:

$$\begin{aligned} p(\mathbf{c}, \mathbf{a}, \sigma, \mathbf{v} | \mathbf{f}; \theta) &\propto p(\mathbf{f} | \mathbf{c}, \mathbf{a}, \sigma, \mathbf{v}, \theta) p(\mathbf{c} | r_c) \\ &\times p(\mathbf{a} | r_a) p(\sigma | r_w) p(\mathbf{v} | r_v) \end{aligned}$$

To sample the posterior distribution, a random walk Gibbs sampler algorithm controlled by a decreasing temperature is used. The principle consists of randomly selecting one of the variables generated by permutation, according to its posterior density. Thus, we randomly and alternately generate "candidate" peak, amplitude, variance and frequency for each class $k \in [1, K]$ and each location n , i.e. the values $(a_{k,n}, c_{k,n}, \sigma_{k,n}, v_{k,n})$. Let us call $\lambda_{k,n}$ a generic parameter representing any of the characteristics $c_{k,n}$, $a_{k,n}$, $\sigma_{k,n}$, $v_{k,n}$ for $n_k \leq n \leq N_k$. Giving the noisy data observation (resp. the modeled data) along the z-axis $\mathbf{f}_x = [f(x, 1), \dots, f(x, M)]^T$ (resp. \mathbf{s}_x), where $x = n$, let us define for each $x \in [1, N]$, the squared norm $\|\mathbf{f}_x - \mathbf{s}_x\|^2$, posterior probability is defined as follows:

$$\begin{aligned} &p\left(\lambda_{k,n} | \mathbf{f}_x, (\lambda_{i,j} \neq \lambda_{k,n})_{1 \leq i \leq K, 1 \leq j \leq N}; \sigma_b, r_\lambda\right) \\ &\propto \exp\left(-\frac{\|\mathbf{f}_x - \mathbf{s}_x\|^2}{2\sigma_b^2} - \frac{\|\mathbf{D}\lambda_k\|}{2r_\lambda}\right) \end{aligned}$$

Thus it is possible to simulate a Metropolis-Hastings algorithm governed by a temperature factor T , searching for the maximum of a posteriori probability (MAP). The algorithm therefore consists of sampling each variable in a random order, conditional on the other variables and the observed data. In other words, let us call for example $\lambda_{k,n}^{(i)}$ the current variable at the iteration i and define, based on (8), the quantities:

$$S(\lambda_{k,n}) = \frac{\|\mathbf{f}_x - \mathbf{s}_x\|^2}{2\sigma_b^2} + \frac{\|\mathbf{D}\lambda_k\|}{2r_\lambda}; W(\lambda_k) = \frac{\|\mathbf{D}\lambda_k\|}{2r_\lambda}$$

where $\mathbf{D}\lambda_k$ takes into account the value $\lambda_{k,n}$. We generate a candidate variable $\tilde{\lambda}_{k,n}$ according to a proposal density, usually defined as a Gaussian distribution in the MCMC approaches in the following way (Kroese et al., 2013):

1. Select a new temperature $T_i \leq T_{i-1}$;
2. Select $\lambda_{k,n}^{(i)}$ randomly among all indexes (k, n) and the corresponding variables $(a_{k,n}^{(i)}, c_{k,n}^{(i)}, \sigma_{k,n}^{(i)}, v_{k,n}^{(i)})$;
3. Generate $\tilde{\lambda}_{k,n}$ according to a proposal density;
4. Keep or reject the candidate value, according to an acceptance probability based on $\frac{S(\tilde{\lambda}_{k,n}) - S(\lambda_{k,n}^{(i)})}{T_i}$;
5. Select randomly an n index (lateral position) and permute the components of the vectors $\lambda_{\mathbf{n}} = (\lambda_{k,n}, \dots, \lambda_{K,n})$ in order to obtain candidate trajectories $(\tilde{\mathbf{a}}_k, \tilde{\mathbf{c}}_k, \tilde{\sigma}_k, \tilde{\mathbf{v}}_k)_{1 \leq k \leq K}$. Reject or accept the new classes on the site n , according to an acceptance probability based on the following distance:

$$\sum_k \sum_{\tilde{\lambda}_k} W(\tilde{\lambda}_k) / T_i - \sum_{\lambda_k} W(\lambda_k) / T_i$$

6. Set $i = i + 1$ and repeat until a stop criterion;

The new parameters $\lambda_{k,n}$ are simulated and their variances r_λ are re-estimated using the classical empirical formula. To initialize the classes k i.e., the information related to the surfaces S_k , and the estimation of the hyper-parameters r_λ , a TKEO based method is used. At each step of the MCMC algorithm, the hyper-parameters are re-estimated by the means of the new estimated parameters $\lambda_{k,n}$. In order to initialize the surfaces, one can take into account their various characteristic parameters: trajectories of the Gaussian centers, their amplitude and variance, as well as the frequencies associated with the local carriers. So it would be possible to discriminate two close surfaces i.e., having close centers, by their amplitudes (a buried transparent layer for example is often of a lower level than the layer of material on the surface). We also take into account a significant number of surface points, i.e., a minimum number of points (at least three pixels). For our study, two main criteria will be able to discriminate surfaces: the minimum relative distance between two neighboring sites and the minimum number of points. Let for example, at the point $(z, n + 1)$, an estimated center z by TK algorithm. Let K be the current number of classes. What we call "class" corresponds to the trajectory of a surface in the 2D image. Then, the membership class k affected to the site will correspond to:

$$k = \begin{cases} \arg \min_{j \in [1, K]} \alpha_j & \text{if } \alpha_j = \left| \frac{z - c_{j,n}}{c_{j,n}} \right| \leq \epsilon, \\ K + 1 & \text{else,} \end{cases} \quad (8)$$

In other words, if a minimal distance α_j relatively to a given class is less than a threshold ϵ (fixed for example at 10%), we take into account the site as belonging to this class j . Otherwise, we declare the site as a new class, provided, however, that there are three successive neighbored sites. Once the classes have been initialize, the variances r_λ are re-estimated using the classic empirical formula computing the variance of initial estimated data $\lambda_{k,n}$. Moreover, we deal with the specific problem of two close surfaces. In order to facilitate the implementation of the Markovian approach, an algorithm based in particular on data compression aims to refine the estimation of the structure of very close surfaces. Indeed, as we will see, in such situations, TK algorithm initialization incorrectly evaluates the surface profiles in this proximity zone. The initial simplifying assumption is based on the local proximity of two surfaces (presence of two materials). Let us consider two close surfaces S_i and S_j according to a criterion of distance, based on the average difference between their respective centers. By means of a run length

coding type compression algorithm, we count the number of close points related to these surfaces, and when these are interrupted by a break zone, suspected of containing adjacent surfaces, we extend the trajectories characteristics in this area. Finally, we present a synopsis of our TK-MCMC method:

Algorithm.

1. Initializes all classes and parameters by TKEO based method using the formulae (2) and a Gaussian approximation of the envelopes along each z axis, providing $\{a_{k,n}, c_{k,n}, \sigma_{k,n}, \nu_{k,n}\}$;
2. Introduce specific initialization of parameters, in adjacent surface regions (see end of section 5);
3. Compute each variance of the trajectories $\forall k$: $r_\lambda = \text{var}(\lambda_k)$ where $\lambda_k = (\lambda_{k,n_1}, \dots, \lambda_{k,n_k})$;
4. Simulate the new parameters $\lambda_{k,n}$ by MCMC;
5. Test the permutation of classes (surfaces) according to the randomly chosen sites $n, 1 \leq n \leq N$;
6. When a criterion has been not reached, go to 3.

6 RESULTS

The proposed model and the robustness of the developed algorithm are illustrated on synthetic and real interferometric signals. Synthetic interferometric signals have been simulated under different "roughness" parameters, i.e., variances r_c according to the Gauss-Markov model presented in section 4, under different SNRs (signal to noise ratio) . The number of classes is set to $K = 2$, then detected automatically by the proposed algorithm. Figures 2, 3 and 4 correspond to the simulation of two surfaces according to different roughness and distances, whereas figure 5 deals with a real interferometric image containing a silicon surface and a buried layer. The corresponding carrier frequencies related to the interferometric signal along the optical axis, take their values around $\nu_0 = 1/320 \text{ nm}^{-1}$ which is a typical physical value. We have indicated in the diagrams, the corresponding normalized pulsations i.e, $\Omega_0 = 2\pi\nu_0 T_e$ where $T_e = 80 \text{ nm}$. Table 1 lists the parameters of the signal relating to the figure 2, i.e. the variance of the noise R , as well as the variances of the parameters related to the trajectories, and their estimated values by our algorithms.

Table 1: Image 1 (Fig. 2): true and estimated parameters R, r_c, r_a, r_w, r_v for TK and MCMC algorithms.

	R	r_c	r_a	r_w	r_v
True value	1	5	$6.25 \cdot 10^{-2}$	$1.31 \cdot 10^{-5}$	$6.17 \cdot 10^{-5}$
Estimated by TK	1.03	1.64	$9.7 \cdot 10^{-2}$	$3.36 \cdot 10^{-5}$	$1.0 \cdot 10^{-3}$
Estimated by MCMC	1.03	4.95	$4.0 \cdot 10^{-2}$	$1.62 \cdot 10^{-5}$	$3.5 \cdot 10^{-5}$

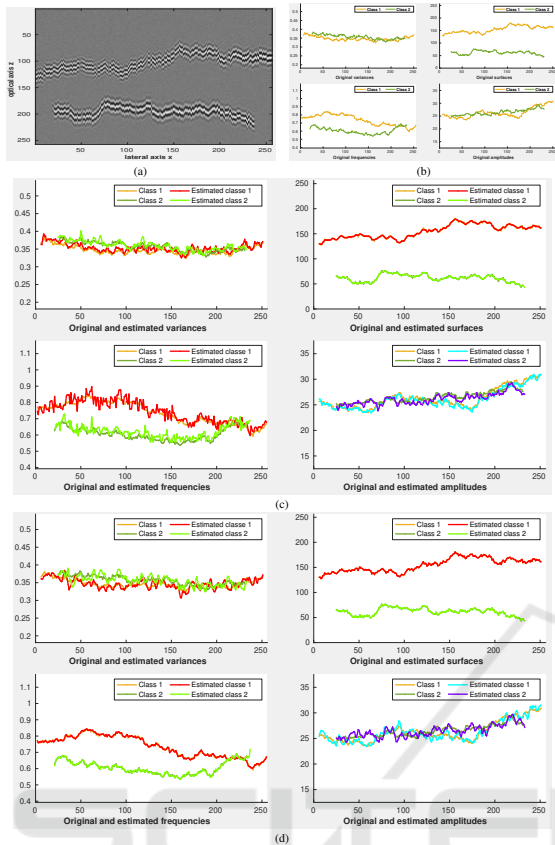


Figure 2: Image 1. (a): Synthetic interferometric signal; (b): true trajectories (from top left to bottom right: variance, surface, frequency, amplitude); (c): estimated trajectories by TK algorithm; (d) estimated trajectories by TK-MCMC.

The value of R corresponds to a SNR fixed to 15 dB. For the parameters r_c , r_a , r_w , r_v , TK-MCMC method improves the estimated values relative to TK method. The estimation of R is identical, since this is based on the variance calculated in a homogeneous area of the initial image. This estimated value therefore does not depend on the method chosen afterward. Table 2 shows the error rates (in percentage) between the original trajectories and the estimated trajectories, concerning the centers, amplitudes, variances and normalized pulsations. It is obvious regarding to these results, that in the specific case of rougher surfaces, TK-MCMC method noticeably improves the error rates. Note that the estimation of the error related to the surfaces is particularly important, since

Table 2: Image 1 (Fig. 2): error rate between true and estimated trajectories for surfaces, amplitudes, variances and frequencies for TK and MCMC algorithms.

	Class 1				Class 2			
	$c_{k,n}$	$a_{k,n}$	$\sigma_{k,n}$	$v_{k,n}$	$c_{k,n}$	$a_{k,n}$	$\sigma_{k,n}$	$v_{k,n}$
TK %	0.76	1.36	1.93	2.91	0.38	1.58	1.59	3.65
MCMC %	0.02	1.13	1.25	0.37	$1.4 \cdot 10^{-2}$	1.14	1.38	0.40

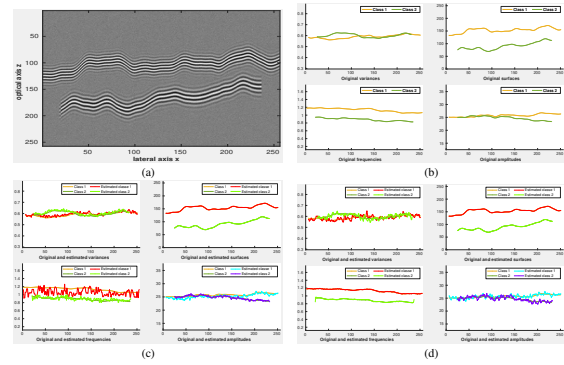


Figure 3: Image 2. (a): Synthetic interferometric signal; (b): true trajectories (from top left to bottom right: variance, surface, frequency, amplitude); (c): estimated trajectories by TK algorithm; (d) estimated trajectories by TK-MCMC.

Table 3: Image 2 (Fig. 3): error rate between true and estimated trajectories for surfaces, amplitudes, variances and frequencies for TK and MCMC algorithms.

	Class 1				Class 2			
	$c_{k,n}$	$a_{k,n}$	$\sigma_{k,n}$	$v_{k,n}$	$c_{k,n}$	$a_{k,n}$	$\sigma_{k,n}$	$v_{k,n}$
TK %	0.09	2.10	1.44	7.84	0.06	0.77	1.35	2.88
MCMC %	0.01	1.71	1.59	0.21	0.01	1.63	1.49	0.25

Table 4: Image 3 (Fig. 4): error rate between true and estimated trajectories for surfaces, amplitudes, variances and frequencies for C-TK and MCMC algorithms.

	Class 1				Class 2			
	$c_{k,n}$	$a_{k,n}$	$\sigma_{k,n}$	$v_{k,n}$	$c_{k,n}$	$a_{k,n}$	$\sigma_{k,n}$	$v_{k,n}$
C-TK %	1.86	17.20	4.39	27.88	1.11	5.78	2.77	12.20
MCMC %	0.02	1.73	2.29	0.24	0.01	1.45	1.82	0.17

it indicates to the shape of surface material. Figure 3(a) represents two smooth surfaces (simulated using Markovian processes whose trajectories were then smoothed by spline functions) and their estimation by both methods (Fig. 3(c)-(d)). The error rates of the corresponding trajectories are reported in Table 3.

Here again, we remark that TK-MCMC algorithm significantly improves the calculation of the parameters (especially the shape of the surfaces i.e., the trajectories of the centers, as well as the estimated frequencies), except for the variance. Figure 4(a) illustrates a situation where two surfaces are close in a region of the interferometric data. Figure 4(b) represents the trajectories estimated by TK algorithm, which fails to connect the surfaces, and introduces parasitic classes.

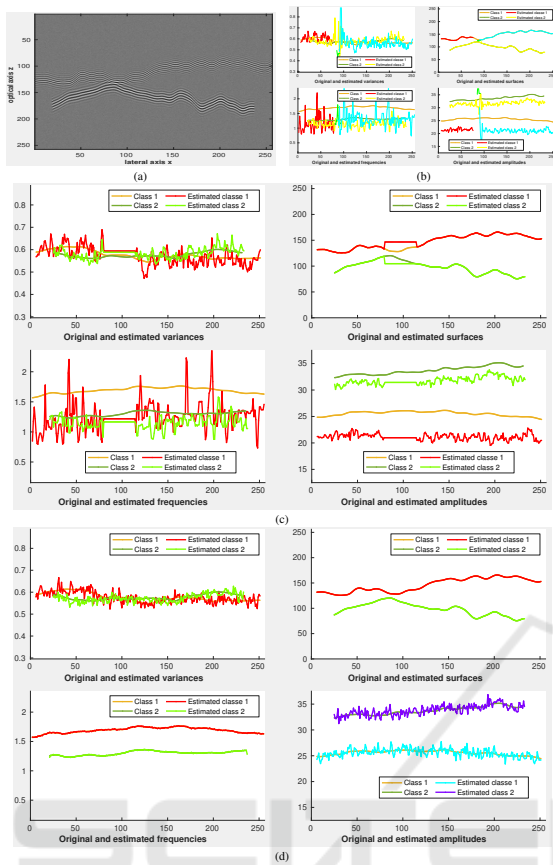


Figure 4: Image 3. (a): Synthetic interferometric signal; (b): estimated trajectories by TK algorithm (surface, amplitude, variance, frequency); (c): corrected estimation by close surfaces algorithm; (d) estimation by MCMC.

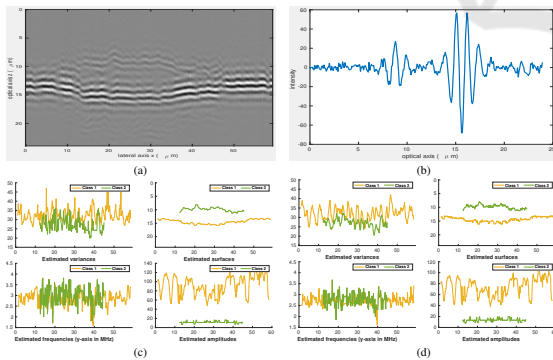


Figure 5: Image 5. (a): Real interferometric signal; (b): profile along the optical axis; (c): estimated trajectories by TK algorithm; (d) estimated trajectories by TK-MCMC.

We show in Figure 4(c) the efficiency of the method stated above taking into account the close surfaces, so as to connect the surfaces, initializing variances, amplitudes and centers around the area of connection, noted by C-TK algorithm. Finally, figure 4(d) illustrates the application of the MCMC method

following this initialization.

According to table 4 and error rates, its effectiveness is clear. Finally figure 5 illustrates the application of our method to a real interferometric signal. We notice in particular that TK and TK-MCMC manage to discriminate well the amplitudes corresponding to the two respective surfaces, which are quite different as shown in figures 5(b). By comparing figure 5(c) and 5(d), TK-MCMC method better homogenizes the values of the carrier frequencies, and more accurately estimates the roughness of the involved surfaces.

7 CONCLUSION

In this article, we have introduced a new method for automatic extraction of material surfaces, combining two types of approaches: a TK nonlinear operator and a Gauss-Markov model introducing a statistical dependence between the surface neighboring points based on four parameters which are able to characterize a fringe signal. This assumption notably makes it possible to extract the homogeneity information by means of the variance parameter. The parameters of the Markovian model, after initialization using TKEO, have been estimated by a MCMC procedure. In the presence of different layers of materials, our method proposes an identification of these, by assigning the points according to a distance criterion. On the other hand, we have studied the case of close surfaces, for which an initialization by the TK algorithm alone is insufficient. In the areas where the points of close surfaces are badly estimated, an algorithm makes it possible to extend the trajectories of these surfaces which are located nearby them. We have numerically illustrated the performance of our method on synthetic and real images, showing an ability to match the roughness of the surfaces. A possible extension of our algorithm could concern on the one hand, upstream an improvement of the initialization by means of a more adapted TK algorithm (for example a higher order one or by using one of the new algorithms as proposed in (Préaux and Boudraa, 2022)). And also an exploitation of the lateral information provided by the neighbored xz sections within a data cube. This would be particularly useful to improve the identification of close surfaces. The complexification of the Markovian model by introducing for instance correlated noise, represents another challenge.

REFERENCES

- Boudraa, A.-O., Cexus, J.-C., Groussat, M., and Brunagel, P. (2008). An energy-based similarity measure for time series. *EURASIP Journal on Advances in Signal Processing*, 2008:1–8.
- Boudraa, A.-O. and Salzenstein, F. (2018). Teager–kaiser energy methods for signal and image analysis: A review. *Digital Signal Processing*, 78:338–375.
- Boudraa, A.-O., Salzenstein, F., and Cexus, J.-C. (2005). Two-dimensional continuous higher-order energy operators. *Optical Engineering*, 44(11):117001–117001.
- Chim, S. S. and Kino, G. S. (1990). Correlation microscope. *Optics Letters*, 15(10):579–581.
- de Groot, P., de Lega, X. C., Kramer, J., and Turzhitsky, M. (2002). Determination of fringe order in white-light interference microscopy. *Applied optics*, 41(22):4571–4578.
- de Groot, P. and Deck, L. (1993). Three-dimensional imaging by sub-nyquist sampling of white-light interferograms. *Optics Letters*, 18(17):1462–1464.
- Gianto, G., Salzenstein, F., and Montgomery, P. (2016). Comparison of envelope detection techniques in coherence scanning interferometry. *Applied Optics*, 55(24):6763–6774.
- Guo, T., Ma, L., Chen, J., Fu, X., and Hu, X. (2011). Microelectromechanical systems surface characterization based on white light phase shifting interferometry. *Optical Engineering*, 50(5):053606–053606.
- Gurov, I., Ermolaeva, E., and Zakharov, A. (2004). Analysis of low-coherence interference fringes by the kalman filtering method. *Journal of the Optical Society of America A*, 21(2):242–251.
- Gurov, I. and Volynsky, M. (2012). Interference fringe analysis based on recurrence computational algorithms. *Optics and Lasers in Engineering*, 50(4):514–521.
- Hissmann, M. and Hamprecht, F. A. (2005). Bayesian surface estimation for white light interferometry. *Optical Engineering*, 44(1):015601–015601.
- Kemao, Q. (2004). Windowed fourier transform for fringe pattern analysis. *Applied Optics*, 43(13):2695–2702.
- Kroese, D. P., Taimre, T., and Botev, Z. I. (2013). *Handbook of Monte-Carlo Methods*. John Wiley & Sons.
- Larkin, K. G. (1996). Efficient nonlinear algorithm for envelope detection in white light interferometry. *Journal of the Optical Society of America A*, 13(4):832–843.
- Larkin, K. G. (2005). Uniform estimation of orientation using local and nonlocal 2-d energy operators. *Optics Express*, 13(20):8097–8121.
- Li, M., Quan, C., and Tay, C. (2008). Continuous wavelet transform for micro-component profile measurement using vertical scanning interferometry. *Optics & Laser Technology*, 40(7):920–929.
- Ma, S., Quan, C., Zhu, R., Tay, C., Chen, L., and Gao, Z. (2011). Micro-profile measurement based on windowed Fourier transform in white-light scanning interferometry. *Optics Communications*, 284(10):2488–2493.
- Maragos, P. and Bovik, A. C. (1995). Image demodulation using multidimensional energy separation. *Journal of the Optical Society of America A*, 12(9):1867–1876.
- Maragos, P., Kaiser, J. F., and Quatieri, T. F. (1993). Energy separation in signal modulations with application to speech analysis. *IEEE Transactions on Signal Processing*, 41(10):3024–3051.
- Maragos, P. and Potamianos, A. (1995). Higher order differential energy operators. *IEEE Signal Processing Letters*, 2(8):152–154.
- Mazet, V., Faisan, S., Awali, S., Gaveau, M.-A., and Poisson, L. (2015). Unsupervised joint decomposition of a spectroscopic signal sequence. *Signal Processing*, 109:193–205.
- Niu, H., Quan, C., and Tay, C. (2009). Phase retrieval of speckle fringe pattern with carriers using 2d wavelet transform. *Optics and Lasers in Engineering*, 47(12):1334–1339.
- O’Mahony, C., Hill, M., Brunet, M., Duane, R., and Mathewson, A. (2003). Characterization of micromechanical structures using white-light interferometry. *Measurement Science and Technology*, 14(10):1807.
- Pavliček, P. and Michalek, V. (2012). White-light interferometry envelope detection by hilbert transform and influence of noise. *Optics and Lasers in Engineering*, 50(8):1063–1068.
- Préaux, Y. and Boudraa, A.-O. (2022). Discrétisation de l’opérateur d’énergie de teager-kaiser revisitée. In *Colloque Grestsi*.
- Préaux, Y., Boudraa, A.-O., and Larkin, K. G. (2022). On the positivity of teager-kaiser’s energy operator. *Signal Processing*, 201:108702.
- Salzenstein, F., Boudraa, A.-O., and Cexus, J.-C. (2007). Generalized higher-order nonlinear energy operators. *Journal of the Optical Society of America A*, 24(12):3717–3727.
- Salzenstein, F., Boudraa, A.-O., and Chonavel, T. (2013). A new class of multi-dimensional teager-kaiser and higher order operators based on directional derivatives. *Multidimensional Systems and Signal Processing*, 24:543–572.
- Salzenstein, F., Montgomery, P., and Boudraa, A.-O. (2014). Local frequency and envelope estimation by teager-kaiser energy operators in white-light scanning interferometry. *Optics Express*, 22(15):18325–18334.
- Sandoz, P. (1997). Wavelet transform as a processing tool in white-light interferometry. *Optics Letters*, 22(14):1065–1067.
- Wu, D. and Boyer, K. L. (2011). Markov random field based phase demodulation of interferometric images. *Computer Vision and Image Understanding*, 115(6):759–770.
- Zhu, P. and Wang, K. (2012). Single-shot two-dimensional surface measurement based on spectrally resolved white-light interferometry. *Applied optics*, 51(21):4971–4975.
- Zou, W., Zhu, L., Wang, W., and Chen, C. (2016). Bayesian denoising of white light interference signal in rough surface measurement. In *MATEC Web of Conferences*, volume 61, page 01002. EDP Sciences.